

## Formate-Mediated Electroenzymatic Synthesis via Biological Cofactor NADH

Wang, Chuanjun; Dong, Wenjin; Zhang, Pengye; Ma, Yaya; Han, Zhiwei; Zou, Yutai; Wang, Wenshuo; Li, Hao; Hollmann, Frank; Liu, Jian

**DOI**

[10.1002/anie.202408756](https://doi.org/10.1002/anie.202408756)

**Publication date**

2024

**Document Version**

Final published version

**Published in**

Angewandte Chemie - International Edition

**Citation (APA)**

Wang, C., Dong, W., Zhang, P., Ma, Y., Han, Z., Zou, Y., Wang, W., Li, H., Hollmann, F., & Liu, J. (2024). Formate-Mediated Electroenzymatic Synthesis via Biological Cofactor NADH. *Angewandte Chemie - International Edition*, 63(41), Article e202408756. <https://doi.org/10.1002/anie.202408756>

**Important note**

To cite this publication, please use the final published version (if applicable).  
Please check the document version above.

**Copyright**

Other than for strictly personal use, it is not permitted to download, forward or distribute the text or part of it, without the consent of the author(s) and/or copyright holder(s), unless the work is under an open content license such as Creative Commons.

**Takedown policy**

Please contact us and provide details if you believe this document breaches copyrights.  
We will remove access to the work immediately and investigate your claim.

***Green Open Access added to TU Delft Institutional Repository***

***'You share, we take care!' - Taverne project***

**<https://www.openaccess.nl/en/you-share-we-take-care>**

Otherwise as indicated in the copyright section: the publisher is the copyright holder of this work and the author uses the Dutch legislation to make this work public.



# Formate-Mediated Electroenzymatic Synthesis via Biological Cofactor NADH

Chuanjun Wang<sup>+</sup>, Wenjin Dong<sup>+</sup>, Pengye Zhang, Yaya Ma, Zhiwei Han, Yutai Zou, Wenshuo Wang,\* Hao Li,\* Frank Hollmann, and Jian Liu\*

*In memoriam of Eberhard Steckhan, an inspiring pioneer of electroenzymology.*

**Abstract:** Synthetic biohybrid systems by coupling artificial system with nature's machinery may offer a disruptive solution to address the global energy crisis. We developed a versatile electroenzymatic pathway for the continuous synthesis of valuable chemicals, facilitated by formate-driven NADH regeneration. Utilizing a bismuth electrocatalyst, we achieved stable CO<sub>2</sub> reduction to formate with approximately 90% Faraday efficiency at a current density of 150 mA cm<sup>-2</sup>. The generated formate acts as a mediator to regenerate NADH, which is then coupled with immobilized redox enzymes—alcohol dehydrogenase (ADH), *L*-lactate dehydrogenase (LDH), and *L*-glutamate dehydrogenase (GDH)—to produce targeted chemicals at significant rates and exceptionally high turnover numbers (1.8×10<sup>6</sup> to 3.1×10<sup>6</sup>). These achievements not only underscore the efficiency of the system but also its practical applicability in industrial settings. By leveraging in situ generated formate, this innovative approach demonstrates the potential of integrating electrocatalysis with enzymatic reactions for sustainable and efficient chemical production on a practical scale.

**E**n route to sustainable, CO<sub>2</sub>-neutral chemical processes electrochemistry represents a key technology.<sup>[1]</sup> If produced from non-fossil sources, electrochemical processes bear an enormous potential for decarbonization. Using electrochemical power to drive biocatalytic redox reactions has also inspired biotechnologists for decades now.<sup>[2]</sup> The vast majority of electroenzymatic processes involve the regener-

ation of either oxidised or reduced nicotinamide cofactors.<sup>[3]</sup> Unfortunately, despite years of intensive investigation by various research groups, current electroenzymatic synthesis still suffer from poor space time yields and overall low product titres making them unattractive for chemical synthesis (Table S1).<sup>[3d,4]</sup>

In the past years, electrochemical CO<sub>2</sub>-reduction (CO<sub>2</sub>R) has been receiving tremendous attention.<sup>[5]</sup> Especially the electrochemical CO<sub>2</sub>R to formate is thermodynamically favourable,<sup>[6]</sup> and exceptionally selective.<sup>[7]</sup> Some proof-of-concept studies have already demonstrated that electrochemically generated formate can serve as carbon- and energy source in electromicrobial conversions.<sup>[8]</sup>

Inspired by these studies, we hypothesized that formate obtained from the electrochemical CO<sub>2</sub>R reaction may also serve as stoichiometric reductant for NADH-dependent enzymatic conversions. To couple formate-reoxidation to NAD<sup>+</sup> reduction, we decided to use the well-known [Cp<sup>\*</sup>Rh(bpy)(H<sub>2</sub>O)]<sup>2+</sup> complex (**M**) because of its versatility and selectivity.<sup>[9]</sup> Overall, an electrochemically-driven, formate-mediated and **M**-catalyzed NADH regeneration system was envisioned to enable biocatalytic reduction reactions (Scheme 1).

Bismuth-based materials have been proved to be efficient electrochemical CO<sub>2</sub>R catalysts with high selectivity to formate and also to have favourable biocompatibility.<sup>[10]</sup> As cathode material for the envisioned electrochemical CO<sub>2</sub>R reaction, we evaluated bismuth-trimesylate metal-organic frameworks (Bi-MOF) and its calcination products (Bi@C-X, X represents the calcination temperature, Figure S1a).

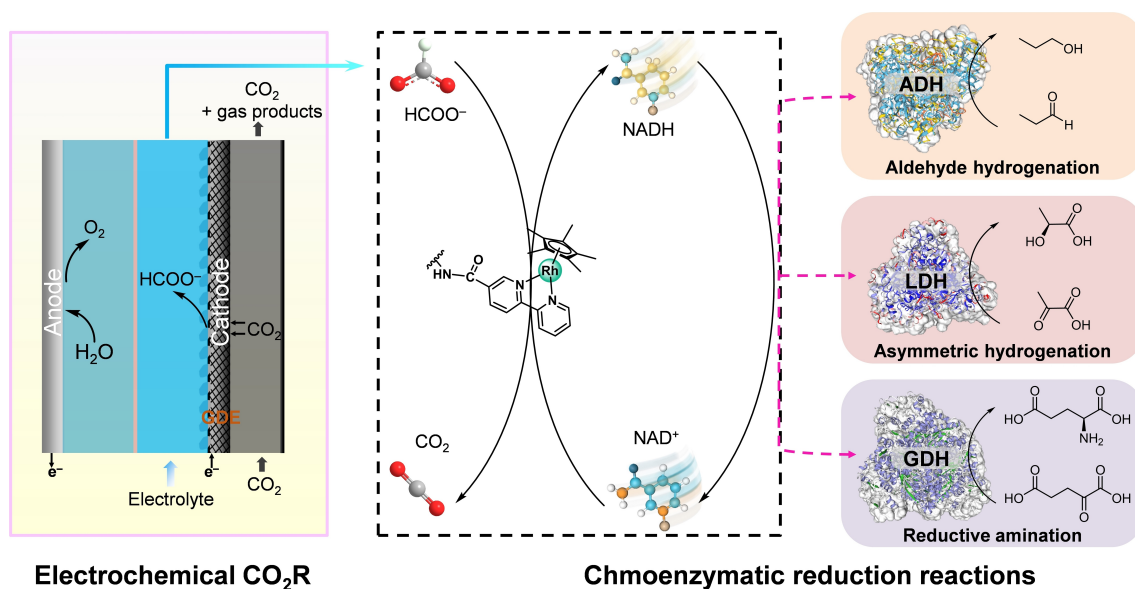
[\*] C. Wang,<sup>+</sup> Dr. H. Li  
 School of Material Science and Engineering  
 Shandong University of Science and Technology  
 Qingdao 266590, China  
 E-mail: lihao89fly@163.com

C. Wang,<sup>+</sup> Dr. W. Dong,<sup>+</sup> P. Zhang, Dr. Y. Ma, Z. Han, Y. Zou,  
 Dr. W. Wang, Prof. J. Liu  
 Key Laboratory of Photoelectric Conversion and Utilization of Solar  
 Energy, Qingdao New Energy Shandong Laboratory,  
 Qingdao Institute of Bioenergy and Bioprocess Technology, Chinese  
 Academy of Sciences  
 Qingdao 266101, China  
 E-mail: wangws@qibebt.ac.cn  
 liujian@qibebt.ac.cn

Y. Zou, Prof. J. Liu  
 College of Materials Science and Engineering  
 Qingdao University of Science and Technology  
 Qingdao 266042, China

Prof. F. Hollmann  
 Department of Biotechnology  
 Delft University of Technology, Delft, The Netherlands

[†] Both authors contributed equally to this work



**Scheme 1.** Schematic representation of the envisioned electrochemically-driven, formate-mediated and **M**-catalyzed NADH regeneration system to enable biocatalytic reduction reactions.

The morphology of the synthesized Bi@C-X samples was analysed using SEM, TEM, and HRTEM techniques. All materials consisted of hexagonal sheets and uniformly distributed nanoparticles (Figure S1b–e and S2a–d). HRTEM suggests a decreasing crystallinity of Bi@C-X with increasing calcination temperature (Figure S2e–j). XRD-, Raman- and XPS- spectroscopy (Figure S3 and S4) reveals the presence of elementary bismuth as well as Bi<sub>2</sub>O<sub>3</sub>. We next investigated the electrochemical properties and CO<sub>2</sub>R activity of the newly prepared electrode materials.

To confirm the CO<sub>2</sub>R performance of the Bi@MOF and Bi@C-X samples, cyclic voltammetry experiments were performed in CO<sub>2</sub>-saturated 0.5 M KHCO<sub>3</sub> electrolyte (Figure S5a–d). All electrode materials exhibited CO<sub>2</sub>R activity with Bi@C-600 standing out due to its high charging current density of 4.46  $\mu\text{F cm}^{-2}$  (Figure S5e), indicating the highest electrochemically active surface area of all materials. In addition, the reaction kinetics of the four samples were determined by electrochemical impedance spectroscopy (EIS) measurements (Figure S6a) and Tafel slope (Figure S6b). With the lowest resistance and the smallest Tafel slope, Bi@C-600 demonstrated superior activity and selectivity for formate production compared to Bi-MOF, Bi@C-500, and Bi@C-700. These analysis results demonstrated that the transformation from Bi-MOF to Bi@C-X increased the effective active sites and enhanced the mass transfer process during CO<sub>2</sub>R. Therefore, we further focused on Bi@C-600 as cathode material for the electrochemical CO<sub>2</sub>R. Pleasingly, undesired products from water reduction (H<sub>2</sub>) or partial CO<sub>2</sub>R (CO) represented only minor by-products in H-cell and the Faradaic efficiency for formate production approached 90% in a wide potential window from –0.8 to –1.4 V versus RHE (Figure 1b), reaching a maximum of 97% at –1.0 V versus RHE. These results further demonstrated that Bi@C-600 outperformed both Bi@C-500 and

Bi@C-700 in the electrochemical reduction of CO<sub>2</sub> to formate (Figure S7).

Furthermore, the CO<sub>2</sub>R performance of the Bi@C-600 catalyst as gas diffusion electrode was tested in a flow cell (Figure 1a), showing excellent activity for CO<sub>2</sub>R to formate with FE<sub>formate</sub> of 92% and current density of 150 mA cm<sup>–2</sup> at –1.61 V versus RHE (Figure 1c). The robustness of the Bi@C-600-catalyzed CO<sub>2</sub>R reaction was confirmed in a long-term chronamperometric experiment, showing no fluctuation or reduction of the current density over at least 20 h of continuous operation and yielding overall 0.65 M of formate (Figure 1d). Also characterization of the catalyst after the experiment (Figure S8 and S9) corroborated its high stability under operational conditions. Finally, also the suitability of the CO<sub>2</sub>R reaction-generated formate to regenerate NADH using **M** as catalyst was demonstrated by UV–vis and NMR spectroscopy (Figure 1e), suggesting exceptionally selective formation of the enzymatically active 1,4-NADH.

Next, we co-immobilized the metalorganic NADH-regeneration catalyst (**M**) with representative, NADH-dependent dehydrogenases (XDH). For this, we chose mesoporous silica to co-immobilize **M** with either alcohol dehydrogenase from *Saccharomyces cerevisiae* (yielding Rh-bpy-MS@ADH), lactate dehydrogenase from rabbit muscle (yielding Rh-bpy-MS@LDH) and glutamate dehydrogenase from bovine liver (yielding Rh-bpy-MS@GDH) (Figure S10a). Restriction of the diffusional mobility of both, **M** and the biocatalysts, not only enabled their use in a plugged-flow reaction setup but also circumvented the frequently observed mutual inactivation of **M** and enzymes.<sup>[11]</sup> The resulting co-immobilizates were characterized intensively using SEM (Figure S10b–e), TEM (Figure S10f) EDS (Figure S10g–i), BET analysis (Figure S11), XRD (Figure S12a), FT-IR spectroscopy (Figure S12b), XPS (Figure S13), conveying a homogeneous distribution of **M** on the surface of

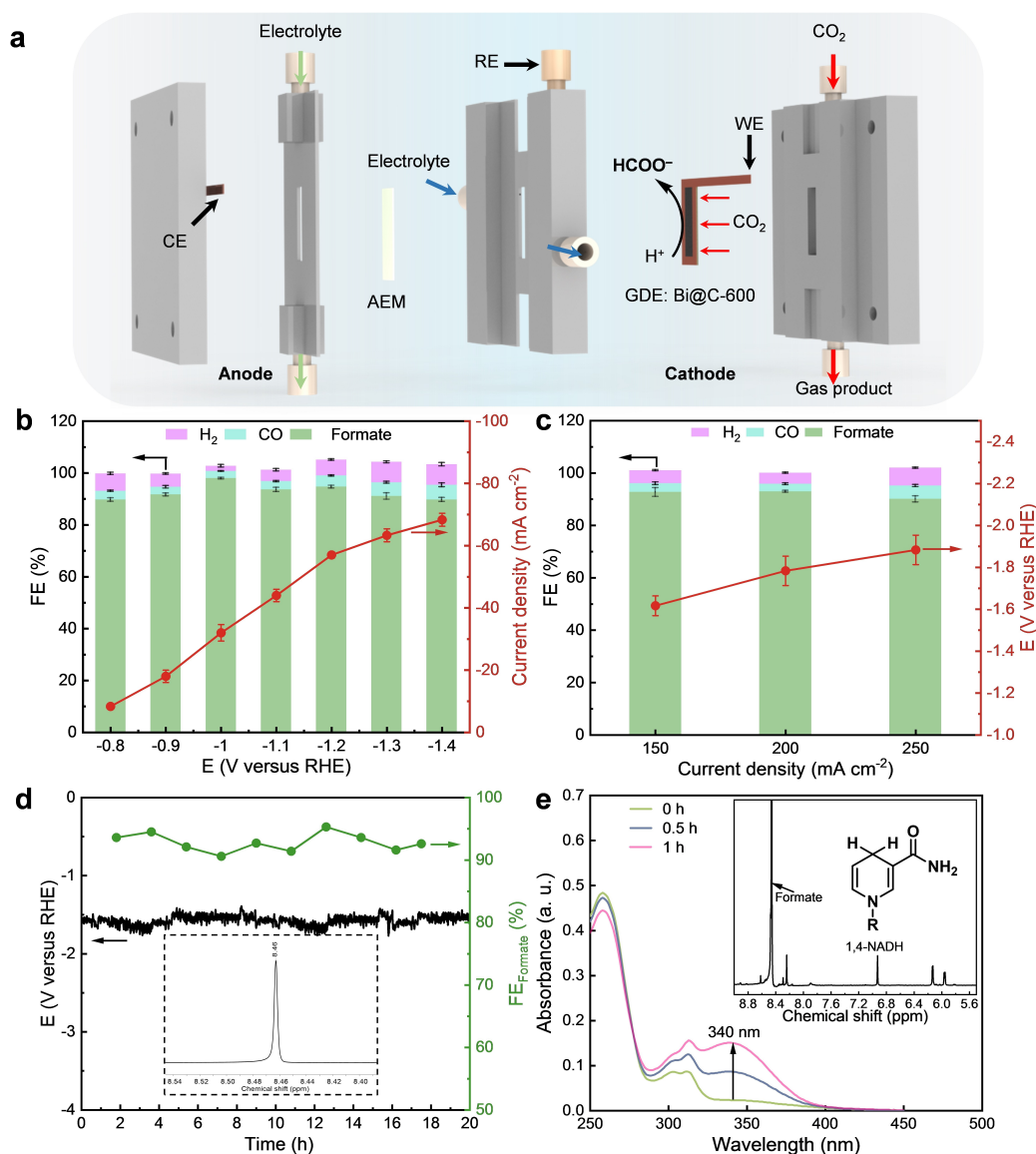


**Figure 1.** Electrocatalytic  $\text{CO}_2\text{R}$  reaction using  $\text{Bi@C-600}$  as electrocatalyst. a) Schematic representation of the flow-through electrolytic cell. The performance and selectivity of the electrochemical formate generation was investigated at different potentials (b) and at different current densities (c). General conditions: 1 h in  $\text{CO}_2$  saturated  $\text{KHCO}_3$  electrolyte. The cell voltage was not compensated by current resistance ( $iR$ ). d) Stability of the  $\text{Bi@C-600}$  catalyst. The reaction was conducted at  $-150 \text{ mA cm}^{-2}$  for 20 h in 0.5 M  $\text{KHCO}_3$  electrolyte. The inset shows a zoom into the  $^1\text{H}$  NMR spectrum of the reaction mixture. e)  $\text{M}$ -catalyzed reduction of  $\text{NAD}^+$  using  $\text{HCOO}^-$  obtained by the  $\text{CO}_2\text{R}$  at  $-150 \text{ mA cm}^{-2}$  in flow cell for 1 h. Reaction conditions: 1 mM  $\text{M}$ , 1 mM  $\text{NAD}^+$ . The inset shows the  $^1\text{H}$  NMR spectrum of the reaction products. The error bars correspond to the standard deviation ( $n=3$ ).

the flower-like, nano-scaled surface. The concentration of  $\text{M}$  on the carrier material was estimated to be 1.44% by inductively coupled plasma mass spectrometry (ICP-MS), corresponding to  $0.14 \text{ mmol g}^{-1}$ . The  $\text{NADH}$  regeneration performance of  $\text{Rh-bpy-MS}$  with different  $\text{Rh}$  contents was evaluated using the  $\text{CO}_2\text{R}$  electrolyte containing formate and compared to the performance of soluble  $\text{M}$  (Figure S14–16). The results reveal that the  $\text{Rh-bpy-MS}$  with a  $\text{Rh}$  content of 1.44% has the best  $\text{NADH}$  regeneration performance and immobilized  $\text{M}$  can afford significant catalytic activity to  $\text{NADH}$  regeneration, achieving 81% conversion rate within 1 h and nearly 100% selectivity

toward 1,4- $\text{NADH}$ . The co-immobilization of redox enzymes was further verified by confocal laser scanning microscopy (CLSM, Figure S17). The enzyme loading for  $\text{Rh-bpy-MS@ADH}$ ,  $\text{Rh-bpy-MS@LDH}$  and  $\text{Rh-bpy-MS@GDH}$  were determined to be  $42.7 \text{ mg g}^{-1}$ ,  $63.5 \text{ mg g}^{-1}$ , and  $63 \text{ mg g}^{-1}$ , corresponding to 0.30, 0.45 and  $0.24 \text{ } \mu\text{mol g}^{-1}$ , respectively (Figure S18).

We next investigated the influence of the formate concentration on the activity of both, the  $\text{NADH}$  regeneration catalyst and of the  $\text{NADH}$ -consuming  $\text{ADH}$  (Figure S19). In line with the previously reported Michaelis–Menten-like dependency of  $\text{M}^{[12]}$  on the formate concen-

trations (c(formate)), we observed a positive correlation between c(formate) and NADH-generation activity (Figure S19a). On the other hand, again in line with the literature<sup>[13]</sup> an inverse relationship was observed for the ADH activity (Figure S19b).

To verify the envisioned dual activity of Rh-bpy-MS@ADH (i.e. formate-driven NADH regeneration and NADH-dependent carbonyl reduction), we compared the overall performance using 'authentic' HCOONa (0.1 M) and CO<sub>2</sub>R-derived formate (Figure 2). Pleasingly, significant product accumulation was observed in all cases. Interestingly, the 'initial' product formation rate was approx. 10 mMh<sup>-1</sup>, which may indicate the NADH-regeneration reaction being overall rate-limiting. Within the 4 h timeframe of these initial experiments, the final concentrations of *n*-propanol, *L*-lactate and *L*-glutamate were 28.6 mM, 36.9 mM and 32.6 mM, respectively. Noteworthy, no significant difference was found between the experiments using

different formate-sources (either electrochemically generated or externally added).

To reveal the mutual inactivation phenomenon of **M** and enzyme and clarify the protection function of the Rh-bpy-MS@XDH, several activity assays were conducted. For formate-driven NADH regeneration system, the addition of enzymes decreased the activity of **M** (Figure S20a). Previously, **M** was reported to deactivate enzymes by binding to nucleophilic amino acid residues.<sup>[14]</sup> In our experiment, after incubated with **M** for 2 hours, free ADH, LDH, and GDH retained about 25.4 %, 15.6 %, and 80.7 % of their original activities, respectively (Figure S20b). It was also found that Rh-bpy-MS@XDH exhibited much better performance for NADH regeneration compared to the mixed samples of Rh-bpy-MS and XDH, indicating that co-immobilization could maintain the activity of **M** (Figure S20c). Similarly, the enzyme activity of Rh-bps-MS@XDH was almost 100 % maintained, confirming that co-immobilization could protect

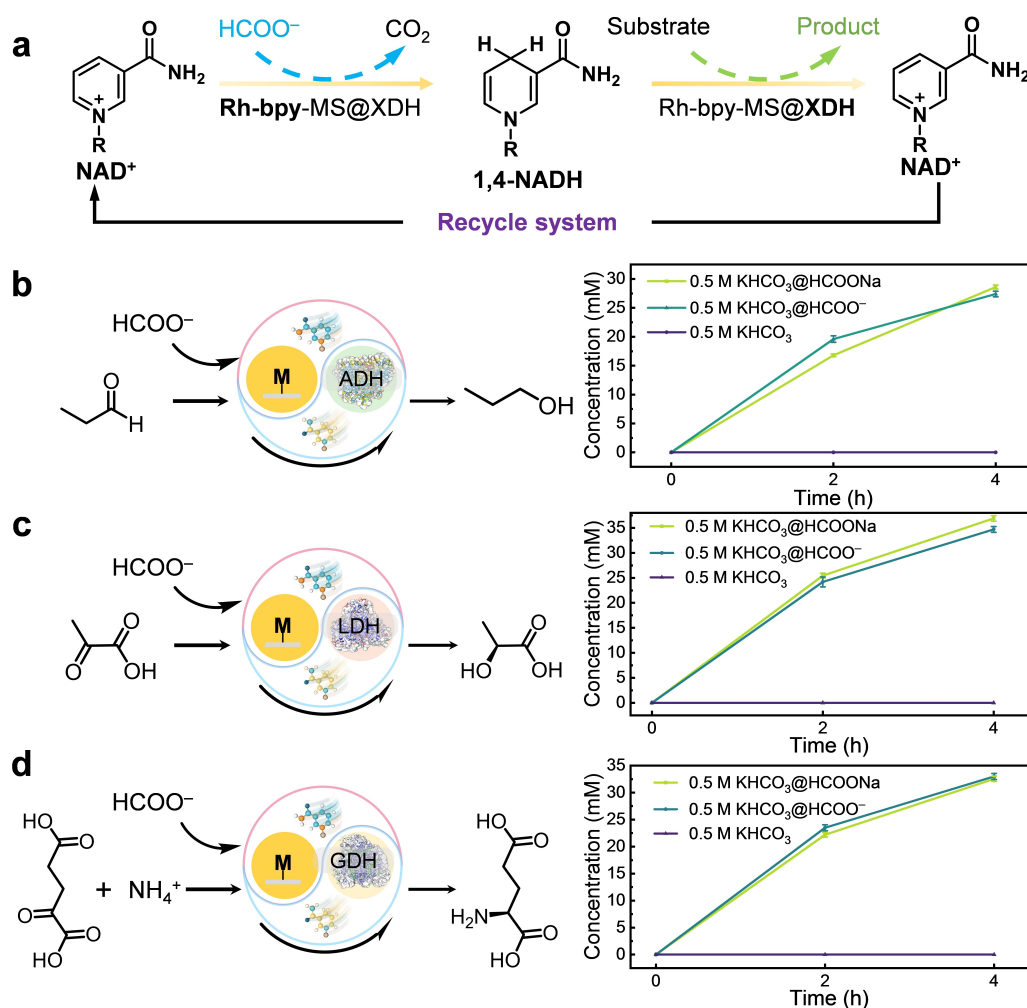


**Figure 2.** Performance of the integrated Rh-bpy-MS@XDH catalysts. a) Schematic illustration of the 1,4-NADH regeneration and the synthesis of different products catalyzed by Rh-bpy-MS@XDH. b) *n*-Propanol synthesis catalyzed by Rh-bpy-MS@ADH in electrolyte with added HCOONa, HCOO<sup>-</sup>, and pure electrolyte, respectively. c) *L*-lactate synthesis catalyzed by Rh-bpy-MS@LDH in electrolyte with added HCOONa, HCOO<sup>-</sup>, and pure electrolyte, respectively. d) *L*-glutamate synthesis catalyzed by Rh-bpy-MS@GDH in electrolyte with added HCOONa, HCOO<sup>-</sup>, and pure electrolyte, respectively. Reaction conditions: HCOONa (0.1 M), HCOO<sup>-</sup> (0.1 M), or pure electrolyte in 4 mL of electrolyte, respectively, 4 mg of Rh-bpy-MS@XDH, 10 mM NAD<sup>+</sup> and 50 mM substrate. The error bars correspond to the standard deviation ( $n = 3$ ).

XDH from deactivation by **M** (Figure S20d). These results indicated co-immobilization systems could retain most of the activity of **M** and XDH by restricting the diffusional freedom of **M** and the biocatalysts.

Finally, we combined the electrochemical CO<sub>2</sub>R reaction with the chemoenzymatic reduction of carbonyl compounds (Figure 3a). The setup consisted of the electrolyzer using a Bi@C-600 gas diffusion electrode and a plugged-flow reactor containing the Rh-bpy-MS@XDH immobilizate; both elements were connected by constant circulation of the aqueous reaction mixture. Since the nicotinamide cofactor was not immobilized, we first confirmed that under the conditions applied no direct cathodic NAD<sup>+</sup> reduction (presumably leading to enzymatically inactive NADH isomers) occurred (Figure S21). Then we tested whether propanal, pyruvate and ketoglutarate could be directly reduced at the cathode. In these control experiments neither a significant reduction of the starting material concentration nor product formation was observed (Figure S22). Throughout the amperostatic electrolyses (input current density of 150 mA cm<sup>-2</sup>), the cathode potential stably remained at -1.6 V vs RHE for at least 24 h (Figure 3b). There was no Bi detectable in the electrolyte (based on ICP-MS analysis), confirming the absence of Bi leaching. Likewise, stable product accumulation was observed and quantified for all three model reactions (Figure S23–26). Importantly, the final product titres for *n*-propanol, *L*-lactate, and *L*-glutamate were 0.472 M, 0.406 M, and 0.370 M, respectively (Figure 3c–e). This corresponds to turnover numbers of

1.8×10<sup>6</sup> to 3.1×10<sup>6</sup> for the biocatalyst. To the best of our knowledge, they are by far the highest product titres and catalyst turnover numbers reported for electroenzymatic transformations (Table S1). It is interesting to note that the formate concentration steadily increased in all experiments indicating that the chemoenzymatic formate-oxidation was overall rate-limiting and that the productivity potential of this setup has not been fully used so far. Besides, the activity and leakage of immobilized enzymes were evaluated during the reaction. The enzyme activity of Rh-bpy-MS@XDH showed a decreasing trend with the increase of time due to the gradual leakage of enzymes (Figure S27). Further study will be conducted to improve the reusability of immobilized enzymes by applying more suitable coatings to immobilized enzymes and using more rigid carrier structures. Additionally, it is worth noting that the reaction system proposed here is nominally CO<sub>2</sub> neutral as the CO<sub>2</sub> emitted during NADH regeneration was previously reduced electrochemically. Provided renewable electricity is used, overall CO<sub>2</sub>-neutrality will be achieved.

Overall, we present a promising electroenzymatic reaction system for carbon-neutral synthesis of value-added chemicals. To the best of our knowledge, the product titres and catalyst performances observed in the current setup exceed those of typical electroenzymatic syntheses by orders of magnitude. A possible reason for this may be that in the current system the NADH-regeneration catalyst (**M**) is not regenerated direct cathodically but indirectly via electrochemically generated formate. Hence, the complex Rh-

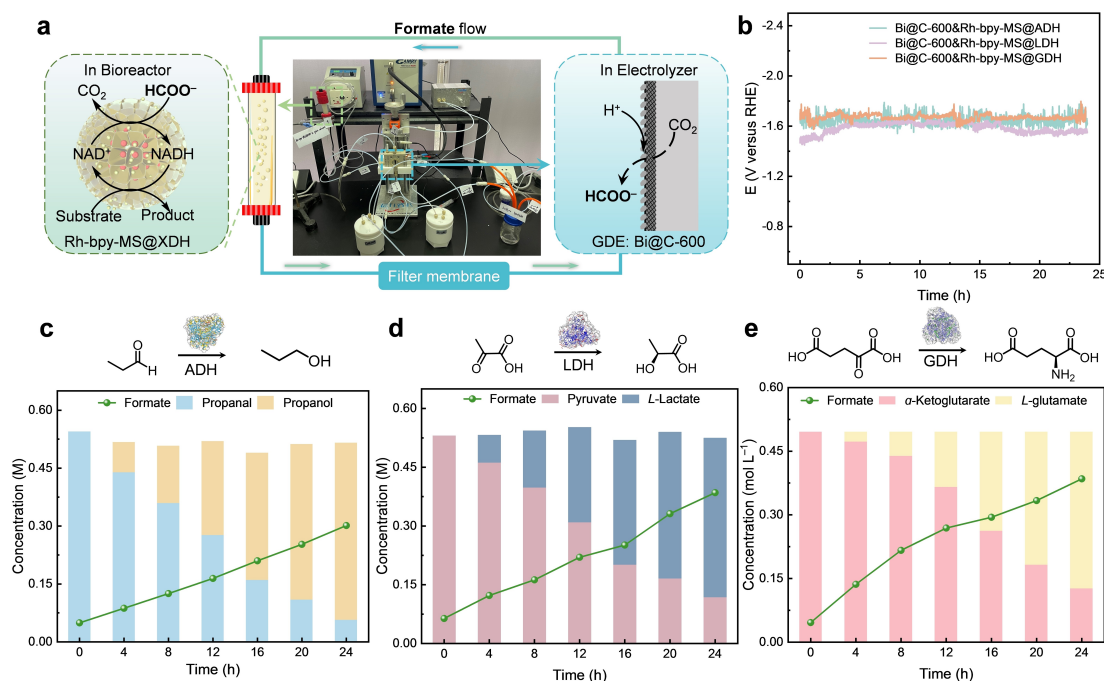


**Figure 3.** Performance of the integrated electroenzymatic system. a) Scheme and photograph of the electroenzymatic system. b) Potential distribution during 24 h of continuous CO<sub>2</sub>R at 150 mA cm<sup>-2</sup>. c) Concentration changes of formate, propanal and *n*-propanol during the catalytic process. d) Concentration changes of formate, pyruvate, and *L*-lactate during the catalytic process. e) Concentration changes of formate,  $\alpha$ -ketoglutarate, and *L*-glutamate during the catalytic process. Reaction conditions: 12.5 mM NAD<sup>+</sup>, 40 mg of the Rh-bpy-MS@XDH, 13 mL min<sup>-1</sup> flow rate, 80 mL total volume.

electrochemistry<sup>[15]</sup> is avoided resulting in more robust processes. The robustness of the production system is further improved by the immobilization of both **M** and the enzymes thereby circumventing their mutual inactivation. Further studies will be necessary to understand the exceptional performance of the proposed reaction system. The proposed system may also prove superior for the electrochemical regeneration of O<sub>2</sub>-dependent monooxygenases where the direct cathodic reduction of O<sub>2</sub> has so far been a major bottleneck.<sup>[2a]</sup> Also extension to more complicated multi-catalytic reaction systems is conceivable. Follow up studies will commence in short due.

## Supporting Information

The authors have cited additional references within the Supporting Information.<sup>[16–26]</sup>

## Acknowledgements

This work was supported by the Natural Science Foundation of Shandong Province (ZR2019ZD47), the National Natural Science Foundation of China (22175104, 22205253), the Education Department of Shandong Province (2019KJC006), Shandong Excellent Young Scientists Fund Program (2023HWYQ-105), the Post-Doctoral Applied Research Project of Qingdao (QDBSH20220202006), the Taishan Scholars Program, and the European Union (ERC, PeroxyZyme, 101054658). Views and opinions expressed are however those of the authors only and do not necessarily reflect those of the European Union or the European Research Council. Neither the European Union nor the granting authority can be held responsible for them.

## Conflict of Interest

The authors declare no conflict of interest.

## Data Availability Statement

The data that support the findings of this study are available from the corresponding author upon reasonable request.

**Keywords:** Electrocatalytic · CO<sub>2</sub> reduction · Electroenzymatic · NADH regeneration · Biosynthesis

- [1] a) P. Zhu, H. Wang, *Nat. Catal.* **2021**, *4*, 943–951; b) J. Li, Y. Zhang, K. Kuruvinnashetti, N. Kornienko, *Nat. Chem. Rev.* **2022**, *6*, 303–319; c) H. Xie, Z. Zhao, T. Liu, Y. Wu, C. Lan, W. Jiang, L. Zhu, Y. Wang, D. Yang, Z. Shao, *Nature* **2022**, *612*, 673–678.
- [2] a) F. Hollmann, A. Schmid, E. Steckhan, *Angew. Chem. Int. Ed.* **2001**, *40*, 169–171; b) S. J. Cobb, S. Rodríguez-Jiménez, E. Reisner, *Angew. Chem. Int. Ed.* **2023**, *63*, e202310547; c) T.

- Zheng, M. Zhang, L. Wu, S. Guo, X. Liu, J. Zhao, W. Xue, J. Li, C. Liu, X. Li, Q. Jiang, J. Bao, J. Zeng, T. Yu, C. Xia, *Nat. Catal.* **2022**, *5*, 388–396; d) J. Kim, J. Jang, T. Hilberath, F. Hollmann, C. B. Park, *Nat. Synth.* **2022**, *1*, 776–786.
- [3] a) F. Hollmann, A. Schmid, *Biocatal. Biotransform.* **2004**, *22*, 63–88; b) R. A. Herold, R. Reinbold, C. J. Schofield, F. A. Armstrong, *Proc. Natl. Acad. Sci. USA* **2023**, *120*, e2214123120; c) S. Kochius, A. O. Magnusson, F. Hollmann, J. Schrader, D. Holtmann, *Appl. Microbiol. Biotechnol.* **2012**, *93*, 2251–2264; d) A. Kurimoto, S. A. Nasser, C. Hunt, M. Rooney, D. J. Dvorak, N. E. LeSage, R. P. Jansonius, S. G. Withers, C. P. Berlinguette, *Nat. Commun.* **2023**, *14*, 1814.
- [4] a) J. A. Bau, A.-H. Emwas, P. Nikolaienko, A. A. Aljarb, V. Tung, M. Rueping, *Nat. Catal.* **2022**, *5*, 397–404; b) S. Kim, M. K. Kim, S. H. Lee, S. Yoon, K.-D. Jung, *J. Mol. Catal., B Enzym.* **2014**, *102*, 9–15; c) Y. Chen, P. Li, H. Noh, C.-W. Kung, C. T. Buru, X. Wang, X. Zhang, O. K. Farha, *Angew. Chem. Int. Ed.* **2019**, *58*, 7682–7686; d) M. Yuan, M. J. Kummer, R. D. Milton, T. Quah, S. D. Minter, *ACS Catal.* **2019**, *9*, 5486–5495; e) W. E. Housseini, M. Etienne, E. Lojou, A. Walcarius, F. Lapique, *Chem. Eng. Process.* **2023**, *187*, 109326.
- [5] a) X. She, L. Zhai, Y. Wang, P. Xiong, M. M.-J. Li, T.-S. Wu, M. C. Wong, X. Guo, Z. Xu, H. Li, H. Xu, Y. Zhu, S. C. E. Tsang, S. P. Lau, *Nat. Energy* **2024**, *9*, 81–91; b) S. Overa, B. H. Ko, Y. Zhao, F. Jiao, *Acc. Chem. Res.* **2022**, *55*, 638–648; c) D. Wakerley, S. Lamaison, J. Wicks, A. Clemens, J. Feaster, D. Corral, S. A. Jaffer, A. Sarkar, M. Fontecave, E. B. Duoss, S. Baker, E. H. Sargent, T. F. Jaramillo, C. Hahn, *Nat. Energy* **2022**, *7*, 130–143; d) J. E. Huang, F. Li, A. Ozden, A. Sedighian Rasouli, F. P. García de Arquer, S. Liu, S. Zhang, M. Luo, X. Wang, Y. Lum, Y. Xu, K. Bertens, R. K. Miao, C.-T. Dinh, D. Sinton, E. H. Sargent, *Science* **2021**, *372*, 1074–1078.
- [6] a) C. W. Lee, N. H. Cho, K. D. Yang, K. T. Nam, *ChemElectroChem* **2017**, *4*, 2130–2136; b) C. Deng, C. Qi, X. Wu, G. Jing, H. Zhao, *Green Carbon* **2024**, *2*, 124–130.
- [7] M. B. Ross, P. De Luna, Y. Li, C.-T. Dinh, D. Kim, P. Yang, E. H. Sargent, *Nat. Catal.* **2019**, *2*, 648–658.
- [8] a) M. Stockl, S. Harms, I. Dinges, S. Dimitrova, D. Holtmann, *ChemSusChem* **2020**, *13*, 4086–4093; b) H. Bi, K. Wang, C. Xu, M. Wang, B. Chen, Y. Fang, X. Tan, J. Zeng, T. Tan, *Chem Catal.* **2023**, *3*, 100557; c) X. Chen, Y. Cao, F. Li, Y. Tian, H. Song, *ACS Catal.* **2018**, *8*, 4429–4437; d) J. Lim, S. Y. Choi, J. W. Lee, S. Y. Lee, H. Lee, *Proc. Natl. Acad. Sci. USA* **2023**, *120*, e2221438120.
- [9] a) R. Ruppert, S. Herrmann, E. Steckhan, *J. Chem. Soc. Chem. Commun.* **1988**, 1150–1151; b) H. C. Lo, O. Buriez, J. B. Kerr, R. H. Fish, *Angew. Chem. Int. Ed.* **1999**, *38*, 1429–1432; c) J. Liu, M. Antonietti, *Energy Environ. Sci.* **2013**, *6*, 1486–1493; d) P. Zhang, W. Dong, Y. Zhang, L.-N. Zhao, H. Yuan, C. Wang, W. Wang, H. Wang, H. Zhang, J. Liu, *Chin. J. Catal.* **2023**, *54*, 188–198; e) G. Lin, Y. Zhang, Y. Hua, C. Zhang, C. Jia, D. Ju, C. Yu, P. Li, J. Liu, *Angew. Chem. Int. Ed.* **2022**, *61*, e202206283.
- [10] a) X.-D. Liang, N. Tian, S.-N. Hu, Z.-Y. Zhou, S.-G. Sun, *Mater. Rep. Energy* **2023**, *3*, 100191; b) Z. Yang, L. Wang, J. Zhang, J. Liu, X. Yu, *Nano Today* **2023**, *49*, 101799.
- [11] T. Himiyama, M. Waki, Y. Maegawa, S. Inagaki, *Angew. Chem. Int. Ed.* **2019**, *58*, 9150–9154.
- [12] F. Hollmann, B. Witholt, A. Schmid, *J. Mol. Catal. B* **2002**, *19–20*, 167–176.
- [13] a) S.-E. Lee, Q. X. Li, J. Yu, *Proteomics* **2006**, *6*, 4259–4268; b) S. Grunwald, A. Mottet, E. Grousseau, J. K. Plassmeier, M. K. Popović, J.-L. Urbelarrea, N. Gorret, S. E. Guillouet, A. Sinskey, *Microb. Biotechnol.* **2015**, *8*, 155–163.
- [14] M. Poizat, I. W. C. E. Arends, F. Hollmann, *J. Mol. Catal. B* **2010**, *63*, 149–156.

- [15] E. Steckhan, S. Herrmann, R. Ruppert, E. Dietz, M. Frede, E. Spika, *Organometallics* **1991**, *10*, 1568–1577.
- [16] a) Y. Kong, X. Jiang, X. Li, J. Sun, Q. Hu, X. Chai, H. Yang, C. He, *Chin. J. Catal.* **2023**, *45*, 95–106; b) P. Pachfule, D. Shinde, M. Majumder, Q. Xu, *Nat. Chem.* **2016**, *8*, 718–724.
- [17] Y. Liang, N. Song, Z. Zhang, W. Chen, J. Feng, B. Xi, S. Xiong, *Adv. Mater.* **2022**, *34*, 2202673.
- [18] J. Phipps, H. Chen, C. Donovan, D. Dominguez, S. Morgan, B. Weidman, C. Fan, H. Beyzavi, *ACS Appl. Mater. Interfaces* **2020**, *12*, 26084–26094.
- [19] Q. Xiao, X. Tao, H. Zou, J. Chen, *Chem. Eng. J.* **2008**, *137*, 38–44.
- [20] Y. Xu, Z. Li, K. Su, T. Fan, L. Cao, *Chem. Eng. J.* **2018**, *341*, 371–382.
- [21] P. Zhan, X. Liu, S. Zhang, Q. Zhu, H. Zhao, C. Ren, J. Zhang, L. Lu, D. Cai, P. Qin, *ACS Appl. Mater. Interfaces* **2023**, *15*, 12855–12863.
- [22] I. N. Chakraborty, V. Jain, P. Roy, P. Kumar, C. P. Vinod, P. P. Pillai, *ACS Catal.* **2024**, *14*, 6740–6748.
- [23] S. Wang, X. Wu, J. Fang, F. Zhang, Y. Liu, H. Liu, Y. He, M. Luo, R. Li, *ACS Catal.* **2023**, *13*, 4433–4443.
- [24] X. Wu, S. Wang, J. Fang, H. Chen, H. Liu, R. Li, *ACS Appl. Mater. Interfaces* **2022**, *14*, 38895–38904.
- [25] J. Liu, X. Ren, C. Li, M. Wang, H. Li, Q. Yang, *Appl. Catal. B* **2022**, *310*, 121314.
- [26] S. Li, Y. Cheng, Y. Chen, J. Li, Y. Sun, J. Shi, Z. Jiang, *Appl. Catal. B* **2022**, *317*, 121772.

Manuscript received: May 8, 2024

Accepted manuscript online: July 22, 2024

Version of record online: September 6, 2024